Failure Prediction Technique for Compression Loaded Carbon Fibre-Epoxy Laminate with Open Holes

C. SOUTIS AND N. A. FLECK
Engineering Department
Cambridge University
Trumpington Street
Cambridge CB2 1PZ
United Kingdom

P. A. SMITH
Department of Materials Science and Engineering
University of Surrey
Guildford, Surrey GU2 5XH
United Kingdom

(Received March 22, 1990)
(Revised September 10, 1990)

ABSTRACT: The inplane compressive fracture behaviour of a carbon fibre-epoxy laminate containing a single hole is examined. Failure is due to 0° fibre microbuckling surrounded by delamination. The microbuckled zone initiates at the hole boundary. It extends stably under increasing load before becoming unstable at a critical microbuckle length of 2–3 mm. The damage propagation and failure of the orthotropic laminate is analysed by a cohesive zone model, in which damage around the open hole is represented by a line crack loaded on its faces. Good agreement between experimental and predicted notched strength is observed for the chosen material and lay-up.

1. INTRODUCTION

EXPERIMENTAL STUDIES HAVE shown that open holes cause a severe reduction in the compressive strength of advanced composite laminates [1,2]. However, the remote failure stress is generally well above the value one might predict from the elastic stress concentration factor, indicating that the composite material is not ideally brittle and some stress relief occurs around the hole. The high stresses at the hole boundary initiate local failures which result in a redistribution of stresses.

Waas and Babcock [3] studied the compressive failure in graphite-epoxy laminates containing a single hole with the aid of real time holographic interferometry and photomicrography. They observed that damage initiates by a combination of fibre microbuckling and delamination. The 0° ply microbuckling originates at the hole edges at 80% of the ultimate compressive strength and propagates into the interior of the specimen. The length of the buckled zone increases with increasing applied load, propagating stably until it reaches a critical length. Then unstable growth begins and the microbuckle traverses the specimen completely.

On an X-ray radiograph the microbuckle resembles a fatigue crack in metals. Due to its crack-like appearance, Guynn et al. [4] compared the damage zone at the edges of the hole to a crack with a plastic zone. They applied the Dugdale model [5] to predict the size of the buckled region as a function of compressive load for both carbon-epoxy and carbon-PEEK composite laminates. In the Dugdale model, the microbuckled region is viewed as a crack loaded on its faces by a constant normal stress, σ. Guynn et al. [4] concluded that a constant stress in the damage zone does not accurately predict the compressive failure stress of the notched laminate and indicates a greater amount of stable microbuckling growth than is observed in practice.

In the current investigation we examine the static compressive behaviour of T800/924C multidirectional specimens containing a single hole. The initiation and growth of damage is explored and a theoretical model is developed for prediction of the notched compressive strength. The damage zone is viewed as a line-crack loaded on its faces by 1) a constant local stress, σ, which is analogous to the yield stress in Dugdale's analysis and 2) a stress which varies linearly with the crack displacement, v: increased damage corresponds to increased crack displacement and to a reduction of the crack face traction.

2. EXPERIMENTAL PROCEDURE

The material used is Toray T800 carbon fibres in a Ciba-Geigy 924C epoxy resin. The preimpregnated tapes were laid-up by hand into 1 m by 0.3 m panels using a $[(\pm 45/0_2)_3]$, stacking sequence and cured according to the manufacturer's recommended procedure at the Royal Aerospace Establishment, Farnborough. Following cure, the laminates were inspected ultrasonically to establish specimen quality and void content.

Specimens of dimensions 245 mm by 50 mm were cut from the 3 mm thick panels, and reinforcement tabs of aluminium were bonded giving a gauge length of 115 mm. Circular holes of diameter 4–15 mm were drilled at the centre of the specimen using a tungsten carbide bit to minimise fibre damage at the hole boundary. In order to obtain the strength and stiffness of the multidirectional material, five unnotched specimens of dimensions 245 mm by 30 mm were cut and end tabs affixed.

Compressive tests were performed on a screw driven machine at a crosshead displacement rate of 0.017 mm s^{-1}. The specimens were loaded by shear action using compressive wedge grips. Guide plates [6] prevented column buckling during compression loading. Considerations of importance throughout the testing procedure were alignment of the specimen in the grips and proper attachment of

0021-9983/91/11 1476-23 $6.00/0

the antibuckling device to the specimen. Strain gauges were bonded to both faces of the specimen remote from any notch; they were used in order to monitor failure strains and to check that there was no significant bending.

Most of the notched specimens were loaded in compression to failure. However, some tests were interrupted prior to catastrophic failure, in order to provide specimens with significant damage for nondestructive examination and sectioning studies [7].

3. TEST RESULTS AND DISCUSSSION

3.1 Unnotched Specimens

The 0° unidirectional compressive properties of the T800/924C composite system were obtained from previous investigation [8] and they are presented in Table 1 together with the compressive properties of the multidirectional $[(\pm 45/0_2)_3]_s$ laminate. The failure strain of the $[(\pm 45/0_2)_3]_s$ plate is almost equal to the failure strain of the 0° laminate indicating that the 45° plies and delamination have little influence on the response of the 0° plies. The failure mode observed is fibre microbuckling [7,8]. The 0° fibres break at two points creating a kink band inclined at an angle $\beta = 5$–$15°$ to the horizontal axis (Figure 1a). The broken fibre segments are 8 to 10 fibre diameters long (~ 50 μm) and rotate by almost 30° from the loading axis. These values are similar to those reported by other investigators [9–11] for carbon fibre–epoxy composites. A schematic representation of the buckling mode is shown in Figure 1b, together with the geometric parameters that define it.

3.2 Specimens with Single Hole

All specimens failed from the hole in a transverse direction to the loading axis, as shown in Figure 2. The failure load decreases as the hole diameter is increased. Results are displayed in Figure 3 where the notched strength σ_n, normalised by the unnotched strength σ_{un} is plotted against the ratio of the hole diameter d to plate width w. Strength values are based on the gross sectional area of the specimen. It is clear from Figure 3 that the strength is decreased by 35–70% by the presence of the hole.

The measured strengths are bounded by simple criteria based on notch sensitivity [12] (Figure 3). If the material is ideally notch insensitive, the failure stress

Table 1. Compressive fracture stress σ_f, failure strain ϵ_f and Young's modulus E_{11}, parallel to 0° fibres. Data is for unnotched specimens in compression.

Lay-Up	σ_F (MPa)	ϵ_F %	E_{11} (GPa)
0°	1615	1.12	161
$[(\pm 45/0_2)_3]_s$	810	1.10	85

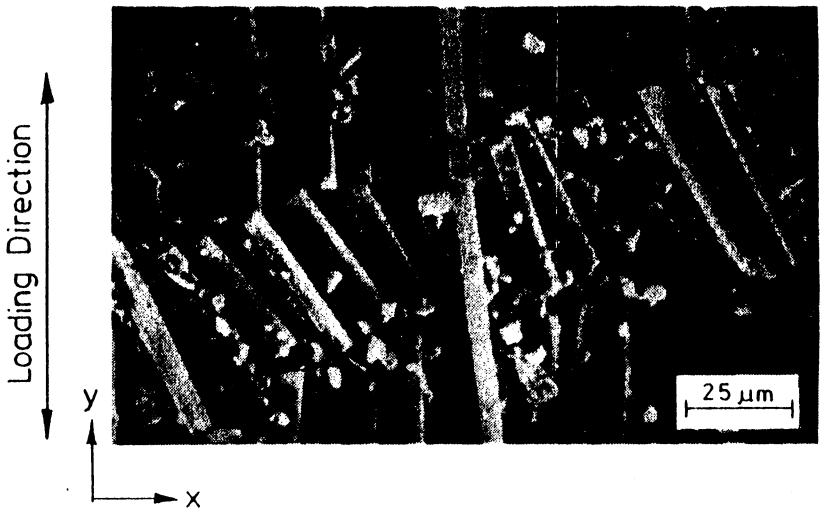

Figure 1a. *Scanning electron photograph showing fibre microbuckling in a T800/924C unnotched unidirectional laminate. Two planes of fracture formed creating a kink band of length equal to 50 μm.*

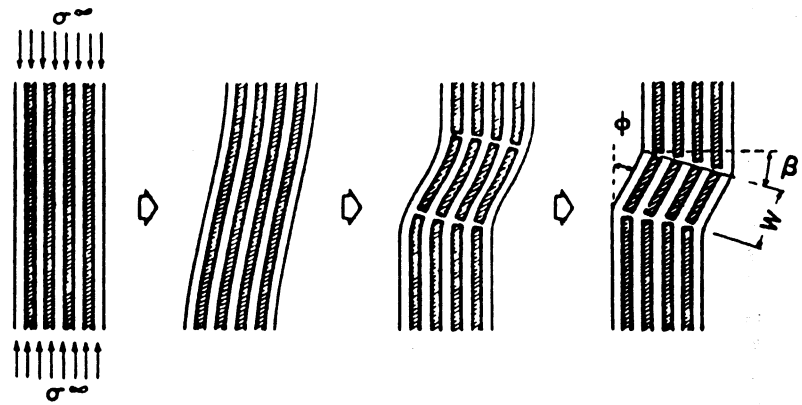

Figure 1b. *A schematic showing the geometry of the 0° buckled fibres (after Evans and Adler [9]).*

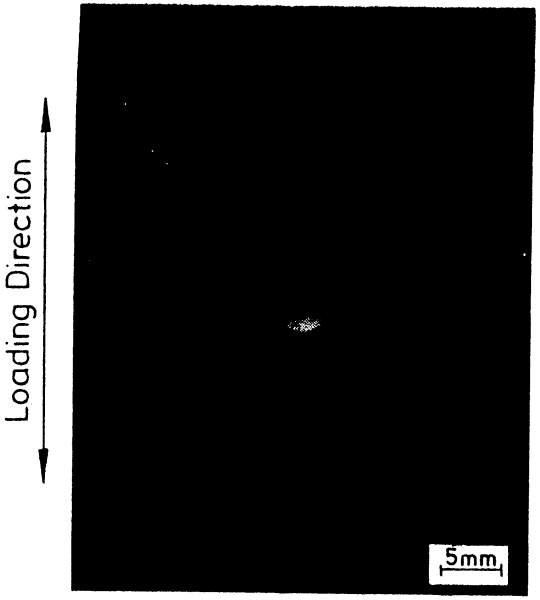

Figure 2. Overall failure of notched specimen showing local delamination, splitting of the 45° plies and fibre breakage (hole diameter = 5 mm).

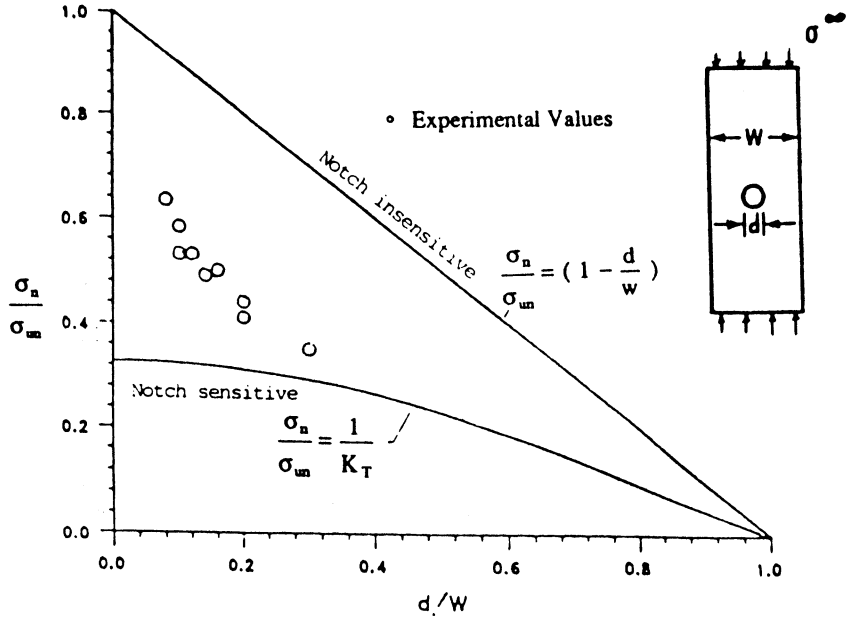

Figure 3. Effect of hole diameter on the strength of the T800/924C composite plate (width = 50 mm).

is proportional to net sectional area, while if the material is ideally notch sensitive then the plate fails when the local stress at the hole edge equals the failure stress of the material. Since the data points lie above the notch sensitive curve, the composite is not ideally brittle and some stress redistribution occurs around the hole before failure. Examination of the damaged specimens reveals that fibre microbuckling in the 0° plies surrounded by delamination occurs in the vicinity of the hole prior to catastrophic failure.

3.3 Damage Mechanisms

Only a brief review of the failure mechanisms in notched laminates is presented here as necessary background to the new theoretical model. A thorough description is given in Reference [7]. The nature and extent of damage in the notched specimens was evaluated by using penetrant enhanced X-ray radiography [13]. At low loads, no damage is evident either on the faces or in the bore of the hole. As the load is increased to 75% of the failure strength 0° splitting occurs at the top and bottom of the hole boundary. The damage becomes more pronounced at about 85% of the specimen's failure load. A typical X-ray photograph taken just before failure is shown in Figure 4a. The damage consists of matrix cracks parallel to the fibres, delamination between the 0° and ±45° layers and fibre microbuckling. Delaminations appear as dark shaded regions and microbuckling as a series of cracks in the radiograph.

The location and nature of damage in individual plies was obtained by using the deply technique [14]. Each ply of the laminate was peeled away and was then examined in the scanning electron microscope. Figure 4b illustrates microbuckling damage in a 0° layer at 85% of the failure load. Fibre microbuckling initiates at the edges of the hole at about 80% of the ultimate strength and occurs first in the

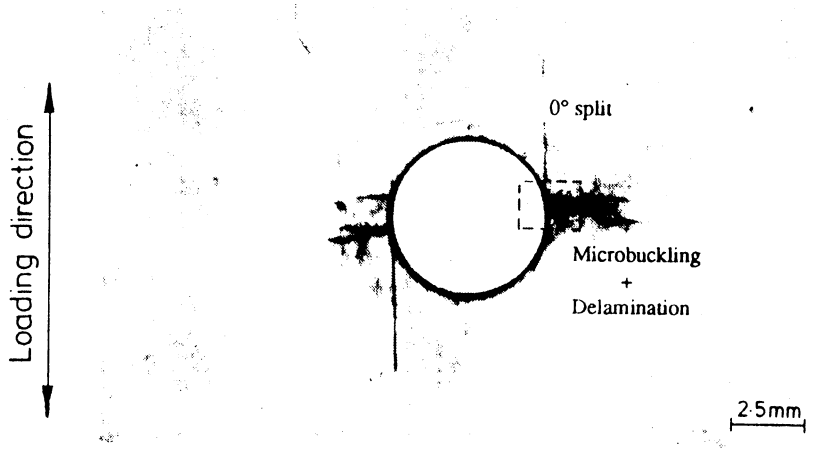

Figure 4a. Fibre microbuckling and delamination emanating from a circular hole at about 95% of failure load. Hole diameter = 5 mm.

Figure 4b. *Magnified view of Figure 4a. Scanning electron photograph showing fibre microbuckling in a 0° ply, in a notched multidirectional laminate.*

outer 0° plies. The 0° fibres buckle into the unsupported hole causing delamination between the 0° and 45° layers (Figure 5a). With increased applied compressive load microbuckling initiates in 0° plies through the thickness of the specimen. Figure 5b was obtained by mechanical polishing and reveals microbuckling in a 0° central ply at 95% of the failure load. The microbuckle is approximately 1.4 mm long and grows almost perpendicular to the loading axis.

In the off-axis plies very little damage was observed. The composite plate fails when microbuckle growth becomes unstable at a microbuckle length of about 2 mm from the hole edge. Because of their greater axial stiffness the 0° layers carry most of the compressive load and hence it is the failure of these laminae which results in laminate fracture.

In the following section the observed damage is modelled as a through-thickness crack loaded on its faces. We assume that the plate is sufficiently thin for plane stress conditions to apply.

4. CRACKED-HOLE SPECIMEN

Mathematically we replace the microbuckle emanating from each side of the hole by a crack. The compressive stress, σ, carried by the microbuckled material is equivalent to a normal traction σ on the crack faces. In addition, the cracked specimen experiences a remote compressive stress, S. It is this remote stress S which drives the microbuckle growth.

We assume that the tractions σ on the crack faces are of sufficient magnitude for the stress intensity factor at the crack tip to vanish. When this condition is satisfied, stresses remain finite everywhere.

The relation between the local compressive stress across the microbuckled layer, σ, and the axial displacement across the layer, $2v$, is not known. The displacement $2v$ is represented by the crack closing displacement (via fibre micro-

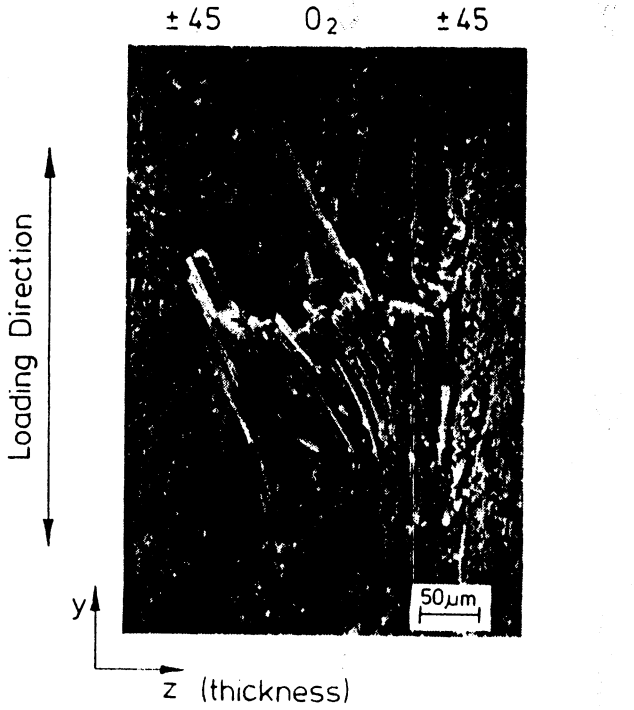

Figure 5a. *Scanning electron micrograph showing the inside bore of the hole. The 0° fibres buckle into the bore of the hole at 80–85% of the failure load.*

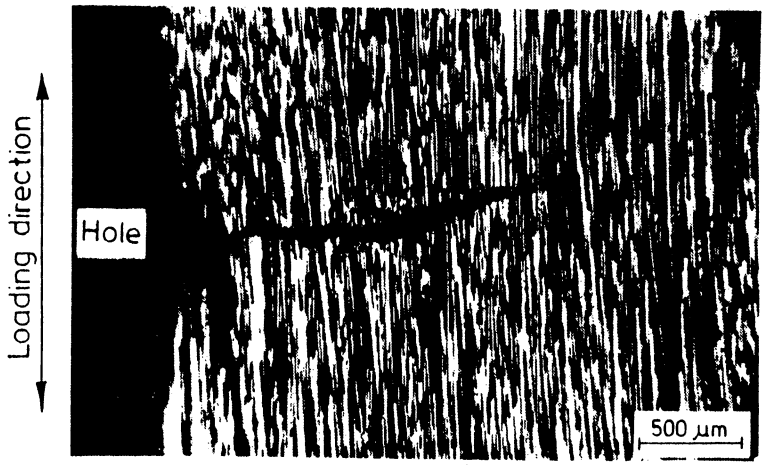

Figure 5b. *Plan view of damage in the central 0° plies. Fibres buckle into the hole. The applied load is 95% of the failure load.*

buckling) profile of the equivalent crack, loaded by the traction σ. We consider two cases:

1. The stress σ across the microbuckled layer, and thus on the crack faces is constant, and independent of v (Figure 6). The crack model is then identical to the Dugdale plastic zone model, where the stress σ represents the yield stress of the material.
2. The stress σ varies linearly with the normal displacement $2v$ across the microbuckle layer (Figure 7).

We consider each case in term.

4.1 Case (1): Constant Crack-Surface Stress

Here, we replace the microbuckle by a crack suffering a constant normal traction σ on its flanks (see Figure 6). The crack length ℓ is determined by requiring that the stress remains finite everywhere. Thus the stress intensity factor, K_{total}, at the ends of the damage zone is zero

$$K_{\text{total}} = K_s + K_\sigma = 0 \tag{1}$$

where K_s and K_σ are the stress intensity factors for a crack emanating from each side of the hole due to the remote stress S and to the local stress σ, respectively.

We consider the superposition of two elastic crack problems; a cracked-hole specimen subjected first to the remote stress, S, and second to a uniform traction, σ, acting over the crack surface. The equations for the stress intensity factors were determined by Newman [15]. The results are as follows.

The stress intensity factor due to the remote stress, S, is equal to

$$K_s = S\sqrt{\pi d}\,F_1F_2 \tag{2}$$

where $d = R + \ell$; R is the hole radius and ℓ is the length of the microbuckled region. The quantities F_1 and F_2 are the boundary-correction factor for the circular hole and finite width, respectively. They are detailed in Appendix A.

The stress intensity factor due to the local stress, σ, is

$$K_\sigma = -\frac{2\sigma}{\pi}\sqrt{\pi d}\left[\frac{\pi}{2} - \sin^{-1}\left(\frac{R}{d}\right)\right]F_3F_4 \tag{3}$$

where the correction factors F_3 and F_4 are given by Equations (A7) and (A10) in Appendix A.

Equations (1-3) may be combined to give

$$S = \sigma\left[1 - \frac{2}{\pi}\sin^{-1}\left(\frac{R}{d}\right)\right]\frac{F_3F_4}{F_1F_2} \tag{4}$$

In general, the correction factors, F_1, F_2, F_3 and F_4 are functions of both material properties and specimen configuration. We neglect the effect of anisotropy on

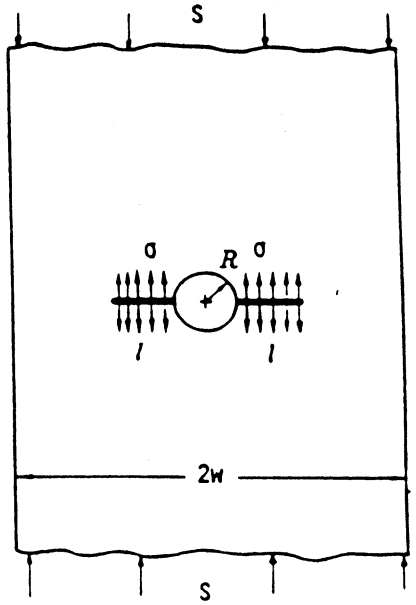

Figure 6. Geometry for the Dugdale model applied to notched composite plate loaded in compression. Local stress, σ, is constant.

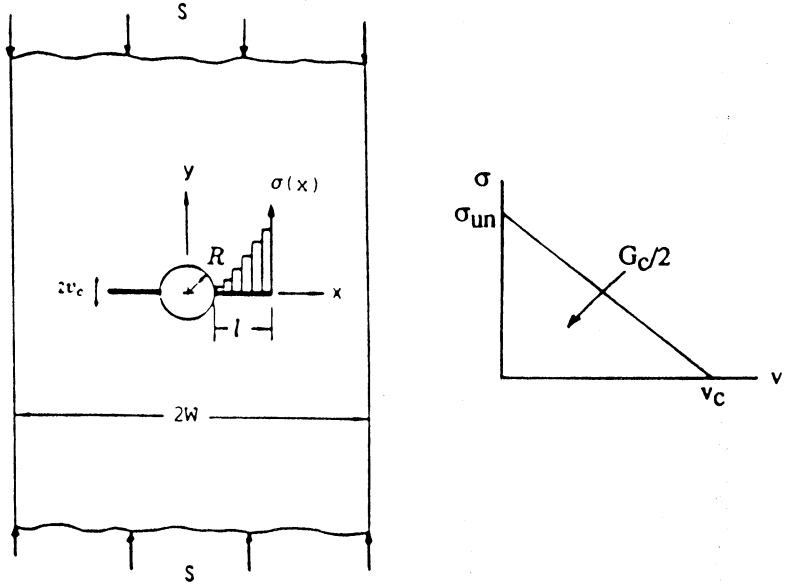

Figure 7. Local stress carried by the buckled zone varies linearly with the vertical displacement.

the correction factors by the following argument. In Reference [7] the stress intensity factor, K, for a centre-cracked tensile (CCT) specimen was calculated using the finite element method. The stress intensity factor calibration was performed for the CCT orthotropic T800/924C, $[(\pm 45/0_2)_3]_s$, laminate with a crack length varying from 10 to 80% of the specimen width. The K values were approximately 2% higher than the values for the isotropic plate of the same geometry. We conclude that the anisotropic effect for the present laminate is small and it can be neglected in the factors F_1, F_2, F_3 and F_4. The quantity σ in Equation (4) represents the stress carried by the broken fibres in the microbuckled zone ℓ. It is assumed implicitly that failed fibres in the damaged zone continue to carry a constant stress σ.

4.1.1 RESULTS

The evolution of microbuckling length ℓ is calculated as a function of remote stress S using Equation (4). Two assumed values are used for σ:

1. The microbuckling stress equals the unnotched strength of the multidirectional laminate, σ = 810 MPa.
2. The stress σ equals the Euler buckling stress

$$\sigma = \left(\frac{\pi d_f}{4w}\right)^2 E_{yy} \tag{5}$$

where d_f is the fibre diameter, w is the kink band width and E_{yy} is the laminate stiffness in the loading direction. Equation (5) assumes that the buckled layer behaves as an Euler strut of length w. This expression was used previously by Weaver et al. [10], and by Hahn et al. [11] to estimate the width w of the buckled zone in unnotched unidirectional laminates. For the $[(\pm 45/0_2)_3]_s$ laminate, E_{yy} = 85 MPa, and w/d_f = 10, giving σ = 525 MPa by Equation (5).

Figure 8a shows the progressive growth of the microbuckled zone under increasing compressive remote stress S, for both values of σ. For σ = 810 MPa, the predicted ultimate failure stress equals 685 MPa, which is much larger than the measured strength of 430 MPa. For σ = 525 MPa, the predicted failure stress equals 445 MPa which compares favourably with the measured strength. However, the model suggests a greater length of stable buckling than is observed, and underestimates the initiation stress for microbuckling. The more sophisticated model, which assumes a linear σ-v response, will be shown to be more accurate on both accounts.

The constant stress model with σ = 525 MPa gives reasonably accurate predictions of the failure strength as a function of hole diameter (see Figure 8b).

4.2 Case (2):Linear σ-v Relationship

For this case we replace the microbuckle by an equivalent crack, such that the normal traction σ on the crack flanks decreases linearly with the crack normal displacement $2v$ (Figure 7).

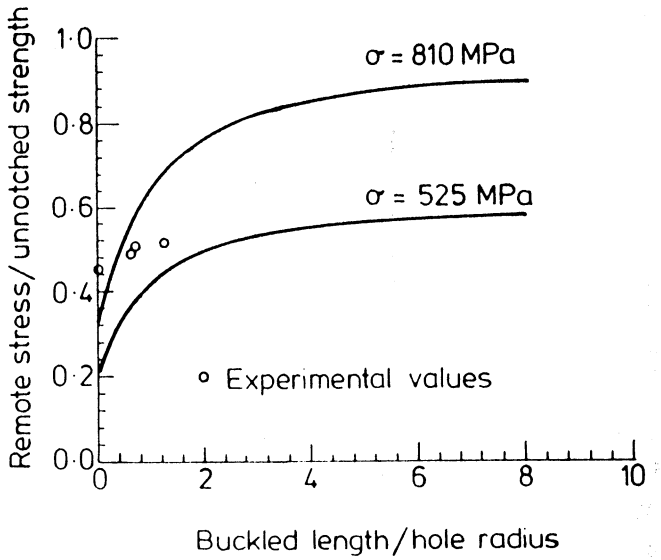

Figure 8a. *Failure strength of T800/924C plate, 50 mm wide with a hole of diameter 5 mm [Equation (4)].*

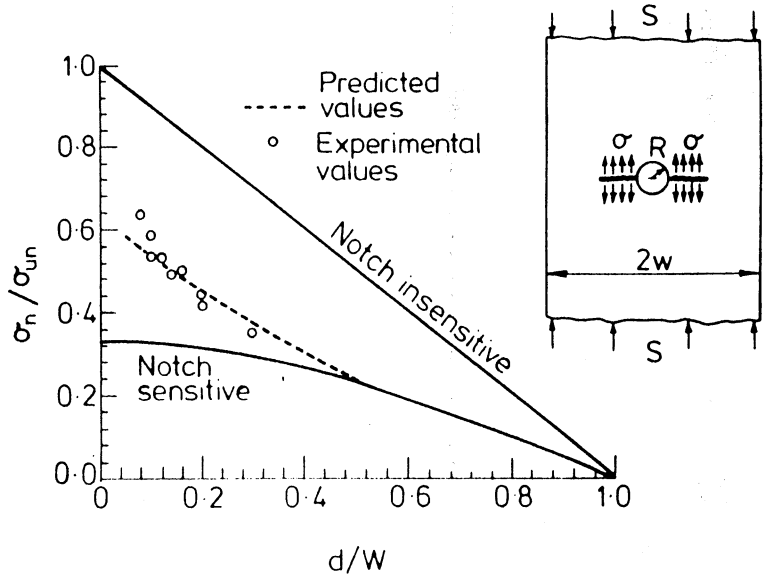

Figure 8b. *Effect of hole diameter on the strength of a 50 mm wide specimen. The prediction is case (a), and assumes a constant microbuckle stress σ = 525 MPa.*

Consider the response of a specimen containing a single hole under an increasing compressive remote load. Initially there is no microbuckling. When the load is increased such that the stress σ_{yy} at the edge of the hole reaches the unnotched compressive strength of the laminate, σ_{un} = 810 MPa, the equivalent crack is formed. By increasing the external load, this crack grows across the specimen's width, thus representing increased damage. As a result of material softening due to damage formation the local stress σ along the crack is assumed to decrease linearly with increasing crack normal displacement, v. The area under the σ-v curve corresponds to the fracture energy G_c

$$G_c = 2\int_0^{v_c} \sigma(v)dv = \sigma_{un} v_c \tag{6}$$

where σ_{un} is the unnotched compressive strength of the laminate and $2v_c$ is the critical crack closing displacement via fibre microbuckling. The toughness G_c represents the total energy dissipated by the microscopic failure processes: fibre microbuckling, matrix plasticity and cracking, and delamination. We measured G_c for the T800/924C, $[(\pm 45/0_2)_3]_s$ laminate by measuring the fracture toughness in compression, using centre cracked specimens. The specimens were 245 mm long by 50 mm wide, and contained central slits pre-sharpened by a razor blade. Results are shown in Figure 9: we find that the measured fracture toughness K_c is independent of crack length, as expected. The fracture energy G_c is related to the fracture toughness K_c by

$$G_c = cK_c^2 \tag{7}$$

where the parameter c is a function of the laminate stiffness matrix, see for example Paris et al. [16]. From a measured value K_c = 46.5 MPa$\sqrt{\text{m}}$, Equation (7) gives G_c = 30 kJ/m^2. Use of the fracture mechanics parameters G_c and K_c is justified since the failure mechanisms operate in a small region near the crack tip compared with other inplane length dimensions.

We calculate the evolution of microbuckling from the edge of the hole in the notched specimens as follows. Damage is represented by an equivalent crack with a linear σ-v relation as shown in Figure 7. The crack is of sufficient length that the stress intensity factor at its tip K_{total} equals zero

$$K_{total} = K_s + K_\sigma = 0 \tag{8}$$

where K_s is given by Equation (2), as before. In order to proceed we discretise the crack into a number n of elements of length $0.025d$. The loading σ on the crack flanks is represented by piecewise constant loading packets, each of magnitude σ_i. As the crack advances, the number of elements n increases.

Consider unit loading on each crack face over the element $\xi = c_i$ to $\xi = b_i$, where ξ is the distance from the crack tip. The stress intensity factor due to this loading is given by the $a_i\sigma_i$, and is defined in Appendix A. For the general case

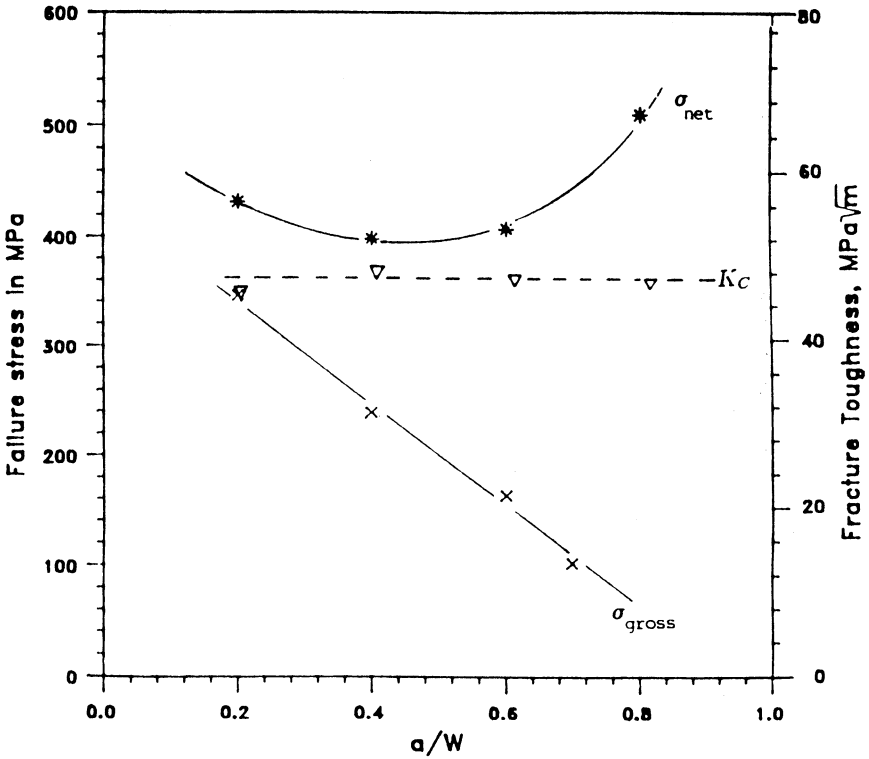

Figure 9. *Failure strength and fracture toughness against (a/W) ratio for a 50 mm wide orthotropic plate.*

of loading by a number of elements on the crack face, K_σ is given by

$$K_\sigma = \sum_{i=1}^{n} a_i\sigma_i \tag{9}$$

After substituting Equations (2) and (9) into Equations (8) and rearranging we find

$$S = \sum_{j=1}^{n} \beta_j\sigma_i \tag{10}$$

where

$$\beta_i = -\frac{2}{\pi}\left[\sin^{-1}\left(\frac{c_i}{d}\right) - \sin^{-1}\left(\frac{b_i}{d}\right)\right]\frac{F_3F_4}{F_1F_2} \tag{11}$$

Equation (10) gives the remote stress S as a function of crack face loading σ_i. In order to calculate σ_i, we consider the crack closing displacement, as follows.

The normal displacement at the midpoint x_i of an element of crack surface is calculated by adding the displacement v_i^s due to the remote stress S and v_i^σ due to local stress σ acting over the damage zone

$$v_i = v_i^s + v_i^\sigma \tag{12}$$

which may be rewritten as

$$v_i = Sf_i + \sum_{j=1}^{n} \sigma_j \alpha_{ij} \tag{13}$$

where f_i and α_{ij} are defined in Appendix A.

Substituting Equation (10) into (13) gives

$$v_i = (f_i\beta_j + \alpha_{ij})\sigma_j \qquad i,j = 1,2,\ldots,n \tag{14}$$

The linear stress-displacement relationship in the damage zone is

$$v_i = v_c\left(I_i - \frac{\sigma_i}{\sigma_{un}}\right) \tag{15}$$

where $I_i \equiv 1$ for all i, and v_c is the critical crack displacement. We calculate v_c from the known values of G_c and σ_{un}, using Equation (6).

Equations (14) and (15) are combined to give an expression for the crack face loading

$$\sigma_j = v_c\left(\frac{v_c}{\sigma_{un}}\delta_{ij} + \alpha_{ij} + f_i\beta_i\right)^{-1} I_i \tag{16}$$

Back substituting σ_j into Equation (10) then gives the remote stress S for any length ℓ of the buckled zone. The plot of S against ℓ shows a maximum S_{max}. When S is equal to the stress S_{max}, the crack (buckle) length has reached a critical value and the laminate fails catastrophically.

4.2.1 RESULTS

The fracture energy G_c and the unnotched compressive strength σ_{un} are taken equal to 30 kJ/m² and 810 MPa, respectively. Equation (6) gives the value for the critical crack displacement $v_c = 37$ μm. The measured vertical displacement associated with fibre rotation in the kink band of Figure 1a is about 7 μm. This discrepancy is due to the fact that delamination and matrix plasticity in the $\pm 45°$ layers contribute to energy dissipation. Predictions are given in Figure 10a, where the ratio of remote stress to unnotched strength is plotted against the ℓ/R for a 5 mm hole specimen. We note that the model underestimates the stress at

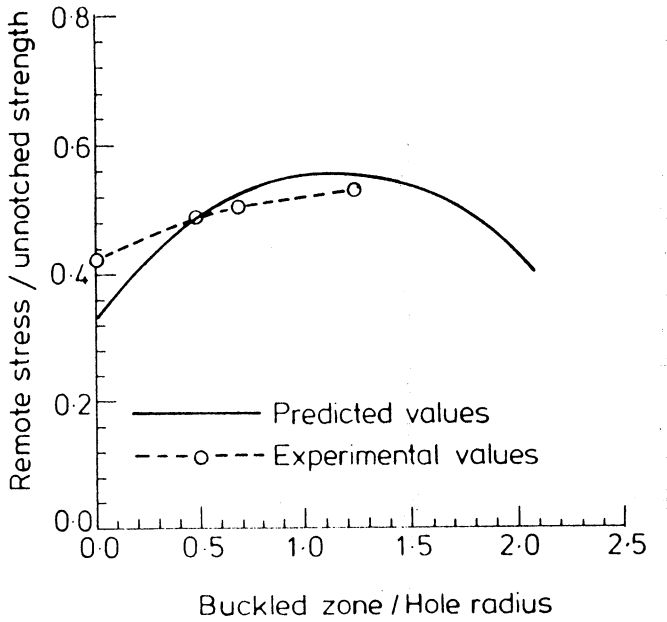

Figure 10a. *Stable damage growth and failure load for a 50 mm wide plate with a 5 mm hole diameter [Equation (10)].*

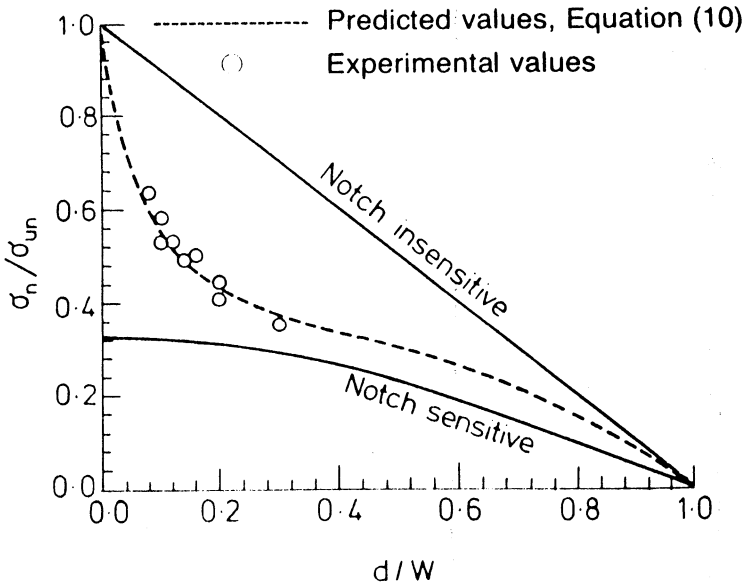

Figure 10b. *Effect of hole diameter on the strength of a plate of width w = 50 mm. The prediction is case (b), where the microbuckle stress varies linearly with crack closing displacement.*

which microbuckling initiates but predicts the critical buckling length and the compressive fracture strength successfully. Predictions of compressive strength are compared with experimental values in Figure 10b, for a range of hole diameters. The agreement is excellent.

5. CONCLUDING REMARKS

Open holes cause more than 40% reduction in the compressive strength of the T800/924C multidirectional laminate. The dominant failure mechanism is fibre microbuckling in the 0° plies surrounded by delamination. The buckle zone initiates at the edges of the hole at 80–85% of the failure load and grows stably under increasing applied load for approximately 2 mm. Then unstable growth begins and catastrophic failure occurs.

The evolution of microbuckling and delamination is predicted with reasonable accuracy when a linear relation is assumed between normal traction on the microbuckle and axial displacement across the microbuckle. The fracture model is relatively simple and relies upon little extra data; it requires a knowledge of the unnotched compressive strength σ_{un} and of the compressive toughness G_c.

The model fails to account for the very early stages of damage growth. This is not surprising since the line model is unable to capture all the details of the complex three-dimensional fracture processes. The next step under current investigation is to test the validity of the model over a range of materials and lay-ups.

ACKNOWLEDGEMENTS

This work was carried out with the financial support of the Procurement Executive of the Ministry of Defence and the Science and Engineering Research Council (SERC). The authors would like to express their appreciation to Dr. P. T. Curtis, from the Royal Aerospace Establishment, Farnborough, for many helpful discussions.

APPENDIX A

1. Dugdale Analysis

In this section a brief description of the Dugdale analysis [5] is presented for a through crack in an infinite isotropic plate, under remote tensile stress S.

The Dugdale model suggests that a crack of length $2a_0$ with a plastic zone of length ℓ can be treated as an effective crack of length $2a$, equal to the sum of $2a_0$ and 2ℓ as in Figure A1(a). The effective crack is subjected to uniform tractions equal to the yield stress of the material, σ_0, applied over the plastic zone and directed such as to pull the crack faces together, as in Figure A1(b); i.e., the material in the plastic zone is assumed to be perfectly plastic.

The length of the plastic zone is selected so that no stress singularity appears at the ends of the extended crack

$$K_s + K_\sigma = 0 \tag{A1}$$

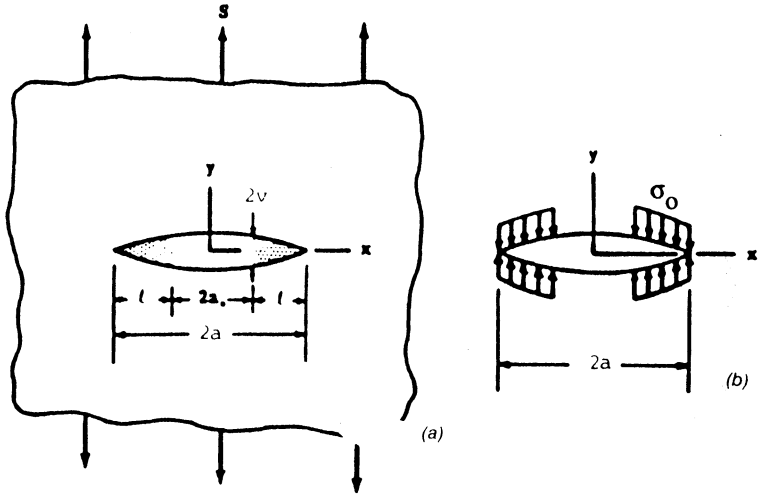

Figure A1. *Dugdale crack configuration: (a) uniform stress S; (b) partially loaded crack.*

where K_s is the stress intensity factor for a crack of length $2a$ in a plate subjected to remote uniform tensile stress, S, and K_σ is the contribution due to crack face loading by a uniform pressure σ_0 over a length ℓ from each crack tip.

Dugdale [5] demonstrated that the plastic zone size for a finite crack in an infinite plate under a remote stress S is given by

$$\ell = a_0 \left(\sec \frac{\pi S}{2\sigma_0} - 1 \right) \tag{A2}$$

2. Newman's Analysis

Newman [15] took the equations for the stress intensity factor and the crack surface displacements, $v(x)$, for a crack subjected to various loadings in an infinite plate from Tada's analysis [17] and modified them for cracks emanating from a circular hole in a finite plate.

2.1 STRESS INTENSITY FACTORS

2.1.1 Remote Uniform Stress

The stress intensity factor for the configuration shown in Figure A2(a) is

$$K_s = S\sqrt{\pi d}\, F_1 F_2 \tag{A3}$$

F_1 is the circular hole correction factor and is given by:

$$F_1 = f\sqrt{1 - \frac{R}{d}} \tag{A4}$$

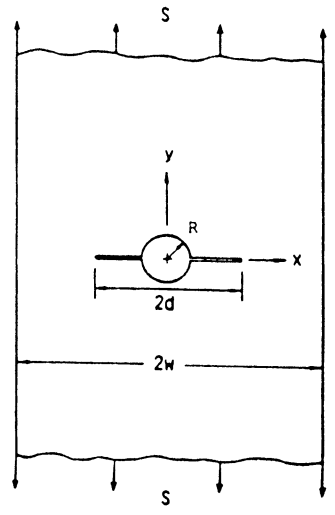

(a) Uniform stress

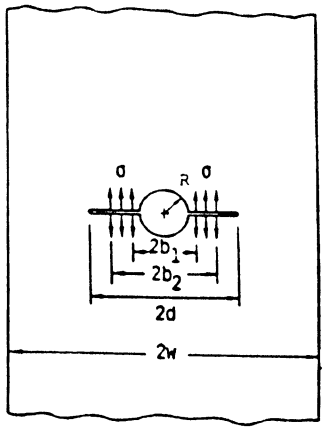

(b) Partially loaded crack

Figure A2. *Cracks emanating from a hole in finite-width plate under various loading.*

where $d = R + \ell$; R is the hole radius and ℓ is the crack length. The function f for two symmetric cracks according to Newman [14] is

$$f = 1 + 0.35\lambda + 1.425\lambda^2 - 1.578\lambda^3 + 2.156\lambda^4 \tag{A4a}$$

with $\lambda = R/d$.

The quantity F_2 is the finite width correction factor and is equal to

$$F_2 = \sqrt{\sec\left(\frac{\pi R}{2W}\right)\sec\left(\frac{\pi d}{2W}\right)} \tag{A5}$$

2.1.2 Partially Loaded Crack

The stress intensity factor for the configuration shown in Figure A2(b) is given by:

$$K_o = \frac{2\sigma}{\pi}\sqrt{\pi d}\left[\sin^{-1}\left(\frac{b_2}{d}\right) - \sin^{-1}\left(\frac{b_1}{d}\right)\right]F_3F_4$$

$$= a\sigma \tag{A6}$$

where the hole correction factor F_3 is

$$F_3 = \frac{G(\gamma,\lambda)}{\left[\sin^{-1}\left(\frac{b_2}{d}\right) - \sin^{-1}\left(\frac{b_1}{d}\right)\right]} \tag{A7}$$

$$G(\gamma,\lambda) = \left\{\left[1 + \frac{A_1}{1-\lambda} + \frac{3A_2}{2(1-\lambda)^2}\right]\sin^{-1}\gamma + \left[\frac{A_1}{(1-\lambda)} + \frac{(4-\gamma)A_2}{2(1-\lambda)^2}\right]\sqrt{1-\gamma^2}\right\}\Bigg|_{\gamma=\frac{b_1}{d}}^{\gamma=\frac{b_2}{d}} \tag{A8}$$

$$A_1 = -0.02\lambda^2 + 0.558\lambda^4$$

$$A_2 = 0.221\lambda^2 + 0.046\lambda^4 \tag{A9}$$

and F_4 is the finite width correction factor given by

$$F_4 = \left[\frac{\sin^{-1}B_2 - \sin^{-1}B_1}{\sin^{-1}\left(\frac{b_2}{d}\right) - \sin^{-1}\left(\frac{b_1}{d}\right)}\right]\sqrt{\sec\left(\frac{\pi d}{2W}\right)} \tag{A10}$$

where

$$B_i = \frac{\sin\left(\frac{\pi b_i}{2W}\right)}{\sin\left(\frac{\pi d}{2W}\right)} \qquad i = 1,2 \tag{A11}$$

When the local stress, σ, on the crack faces is piecewise constant along the crack flanks the same formulae are applied as above with b_1 and b_2 replaced by b_i and c_i, respectively, where

$$c_i = (R + \ell) - \left(\frac{i-1}{n}\right)\ell$$
$$b_i = (R + \ell) - \frac{i}{n}\ell \tag{A12}$$

for $i = 1,2,\ldots n$.

2.2 CRACK-SURFACE DISPLACEMENTS

2.2.1 Remote Uniform Stress

The approximate crack surface displacements for the problem in Figure A2(a) for a finite plate are:

$$v_s = \frac{2S}{E}\sqrt{d^2 - x^2}F_1F_2$$
$$= fS \qquad |x| \le d \tag{A13}$$

When the traction along the crack faces is represented in a piecewise constant fashion the displacement v_s at the midpoint of each loading element x_i is

$$v_s = \frac{2S}{E}\sqrt{d^2 - x_i^2}F_1F_2 \tag{A13a}$$

where

$$x_i = (R + \ell) - \left(\frac{i - 1/2}{n}\right)\ell \tag{A13b}$$

2.2.2 Partially-Loaded Crack

The approximate crack surface displacements for the loading shown in Figure A2(b) are

$$v_o = [v_o^\infty(x) + v_o^\infty(-x)]F_3F_4 \tag{A14}$$

where

$$v_o^\infty(x) = \frac{2\sigma}{\pi E}\left[(b - x)\cosh^{-1}\left(\frac{d^2 - bx}{d|b - x|}\right) + \sqrt{d^2 - x^2}\sin^{-1}\left(\frac{b}{d}\right)\right]\Bigg|_{b=b_1}^{b=b_2} \tag{A15}$$

for $|x| \le d$.

The factors F_3 and F_4 are given by Equations (A7) and (A10), respectively.

The displacement v_i^σ at a point x_i in the damage zone due to a unit stress over a loading packet centred at x_j may be written as

$$v_i^\sigma = \alpha_{ij}\sigma_j \tag{A16}$$

where

$$\alpha_{ij} = A(x_i, x_j) + A(-x_i, x_j) \tag{A17}$$

The function $A(x_i, x_j)$ is given by Equation (A15) with $b_1 = b_j$ and $b_2 = c_j$ for $j = 1,2,\ldots,n$. For plane stress A is

$$A(x_i, x_j) = \frac{2}{\pi E}\left\{(c_j - x_i)\cosh^{-1}\frac{d^2 - c_jx_i}{d|x_i - c_j|} - (b_j - x_i)\cosh^{-1}\frac{d^2 - b_jx_i}{d|x_i - b_j|}\right.$$
$$\left. + \sqrt{d^2 - x_i^2}\left[\sin^{-1}\left(\frac{c_j}{d}\right) - \sin^{-1}\left(\frac{b_j}{d}\right)\right]\right\}F_3F_4 \tag{A18}$$

for $i,j = 1,2,\ldots,n$.

REFERENCES

1. Starnes, J. H., M. D. Rhodes and J. G. Williams. 1979. "Effect of Impact Damage and Holes on the Compressive Strength of Graphite/Epoxy Laminates," *Nondestructive Evaluation and Flaw Criticality of Composite Materials, ASTM STP 696*, pp. 147–171.
2. Rhodes, M. D., M. M. Mikulas and P. E. McGowan. 1984. "Effects of Orthotropy and Width on the Compression Strength of Graphite/Epoxy Panels with Holes," *AIAA Journal*, 22(9): 1283–1292.
3. Waas, A. and Babcock. 1986. "Observation of the Initiation and Progression of Damage in Compressively Loaded Composite Plates Containing a Cutout," NASA Progress Report, Grant NSG-1483.
4. Guynn, E. G., W. L. Bradley and W. Elber. 1989. "Micromechanics of Compression Failures in Open Hole Composite Laminates," *Composite Materials: Fatigue and Fracture, ASTM STP 1012*, pp. 118–136.
5. Dugdale, D. S. 1960. "Yielding of Steel Sheets Containing Slits," *J. Mechanics and Physics of Solids*, pp. 100–104.
6. Curtis, P. T. 1985. "CRAG Test Methods for the Measurement of the Engineering Properties of Fibre Reinforced Plastics," RAE TR-85099.

7. Soutis, C. and N. A. Fleck. 1990. "Static Compression Failure of Carbon Fibre T800/924C Composite Plate with a Single Hole," *J. Composite Materials*, 24:536–558.
8. Soutis, C., P. A. Smith and N. A. Fleck. 1988. "Investigation of Notched Compressive Strength of Carbon Fibre Reinforced Plastics," *Phase Interaction in Composite Materials, 2nd International Symposium, Patras, Greece*.
9. Evans, A. G. and W. F. Adler. 1977. "Kinking as a Mode of Structural Degradation in Carbon Fibre Composites," *Acta Metallurgica*, 26(5):725–738.
10. Weaver, C. W. and J. G. Williams. 1975. "Deformation of Carbon-Epoxy Composite under Hydrostatic Pressure," *J. Materials Science*, 10:1323–1333.
11. Hahn, H. T. and J. G. Williams. 1984. "Compression Failure Mechanisms in Unidirectional Composites," NASA TM-85834.
12. Mikulas, M. M. 1980. "Failure Prediction Techniques for Compression Loaded Composite Laminates with Holes," NASA CP-2142.
13. Scott, I. G. and C. M. Scala. 1982. "A Review of Non-Destructive Testing of Composite Materials," *NDT International*, 12:75.
14. Freeman, S. M. 1982. "Characterization of Laminar and Interlaminar Damage in Graphite/Epoxy Composites by Deply Technique," *Composite Materials; Testing and Design (6th Conference, ASTM STP 787*, pp. 50–62.
15. Newman, J. C. 1982. "A Nonlinear Fracture Mechanics Approach to the Growth of Small Cracks," *Behavior of Short Cracks on Airframe Components, AGARD Conf. Proc., France*.
16. Paris, P. C. and G. C. Sih. 1969. "Stress Analysis of Cracks," *Fracture Toughness Testing and Its Implications, ASTM STP 381*, pp. 30–83.
17. Tada, H., P. C. Paris and G. R. Irwin. 1973. *The Stress Analysis of Cracks Handbook*. St. Louis, MO: Del Research Corporation.